

Delivery of temozolomide and N3-propargyl analog to brain tumors using an apoferritin nanocage

kaouthar Bouzinab, helen summers, Malcolm F.G. Stevens, Christopher J. Moody, Neil Rodney Thomas, Pavel Gershkovich, nicola weston, Marianne B. Ashford, Tracey D Bradshaw, and Lyudmila Turyanska

ACS Appl. Mater. Interfaces, **Just Accepted Manuscript** • DOI: 10.1021/acsami.0c01514 • Publication Date (Web): 19 Feb 2020

Downloaded from pubs.acs.org on February 20, 2020

Just Accepted

“Just Accepted” manuscripts have been peer-reviewed and accepted for publication. They are posted online prior to technical editing, formatting for publication and author proofing. The American Chemical Society provides “Just Accepted” as a service to the research community to expedite the dissemination of scientific material as soon as possible after acceptance. “Just Accepted” manuscripts appear in full in PDF format accompanied by an HTML abstract. “Just Accepted” manuscripts have been fully peer reviewed, but should not be considered the official version of record. They are citable by the Digital Object Identifier (DOI®). “Just Accepted” is an optional service offered to authors. Therefore, the “Just Accepted” Web site may not include all articles that will be published in the journal. After a manuscript is technically edited and formatted, it will be removed from the “Just Accepted” Web site and published as an ASAP article. Note that technical editing may introduce minor changes to the manuscript text and/or graphics which could affect content, and all legal disclaimers and ethical guidelines that apply to the journal pertain. ACS cannot be held responsible for errors or consequences arising from the use of information contained in these “Just Accepted” manuscripts.

1
2
3
4
5
6
7
8
9
10
11
12
13
14
15
16
17
18
19
20
21
22
23
24
25
26
27
28
29
30
31
32
33
34
35
36
37
38
39
40
41
42
43
44
45
46
47
48
49
50
51
52
53
54
55
56
57
58
59
60

Delivery of temozolomide and N3-propargyl analog to brain tumors using an apoferritin nanocage

*Kaouthar Bouzinab^a, Helen S. Summers^b, Malcolm F. G. Stevens^a, Christopher J. Moody^b,
Neil R. Thomas^c, Pavel Gershkovich^a, Nicola Weston^d, Marianne B. Ashford^e,
Tracey D. Bradshaw^{a*} and Lyudmila Turyanska^{f*}*

^aBiodiscovery Institute, School of Pharmacy, University of Nottingham, NG7 2RD, UK.

^bSchool of Chemistry, University of Nottingham, NG7 2RD, UK.

^cBiodiscovery Institute, School of Chemistry, University of Nottingham, NG7 2RD, UK.

^dNanoscale and Microscale Research Centre, University of Nottingham, NG7 2RD, UK.

^eAdvanced Drug Delivery, Pharmaceutical Sciences, R & D, AstraZeneca, Macclesfield, UK.

^fFaculty of Engineering, University of Nottingham, NG7 2RD, UK

CORRESPONDING AUTHORS: Tracey.Bradshaw@nottingham.ac.uk

Lyudmila.Turyanska@nottingham.ac.uk

KEYWORDS: Temozolomide; Apoferritin; Glioblastoma multiforme; Drug delivery system.

This work was supported by the Engineering and Physical Sciences Research Council [grant number EP/L01646X/1; EP/L022494/1; EP/P03/1684/1] and the EPSRC Centre for Doctoral Training in Advanced Therapeutics and Nanomedicines

1
2
3 ABSTRACT
4

5 Glioblastoma multiforme (GBM) is a grade IV astrocytoma, which is the most aggressive form
6 of brain tumor. The standard of care for this disease includes surgery, radiotherapy and
7 temozolomide (TMZ) chemotherapy. Poor accumulation of TMZ at the tumor site, tumor
8 resistance to drug and dose-limiting bone marrow toxicity eventually reduce the success of this
9 treatment. Herein, we have encapsulated > 500 drug molecules of TMZ into the biocompatible
10 protein nanocage, apoferritin (AFt), using a 'nanoreactor' method (AFt-TMZ). AFt is
11 internalized by transferrin receptor 1-mediated endocytosis and is therefore able to facilitate
12 cancer cell-uptake and enhance drug efficacy. Following encapsulation, the protein cage
13 retained its morphological integrity and surface charge, hence its cellular recognition and
14 uptake are not affected by the presence of this cargo. Additional benefits of AFt include
15 maintenance of TMZ stability at pH 5.5 and drug release under acidic pH conditions,
16 encountered in lysosomal compartments. MTT assays revealed that the encapsulated agents
17 displayed significantly increased anti-tumor activity in U373V (vector control) and,
18 remarkably the isogenic, U373M (MGMT expressing TMZ-resistant) GBM cell lines, with
19 GI_{50} values < 1.5 μ M for AFt-TMZ, compared to 35 μ M and 376 μ M for unencapsulated TMZ
20 against U373V and U373M, respectively. The enhanced potency of AFt-TMZ was further
21 substantiated by clonogenic assays. Potentiated G2/M cell cycle arrest following exposure of
22 cells to AFt-TMZ indicated an enhanced DNA damage burden. Indeed, increased O6-
23 methylguanine (O6-MeG) adducts in cells exposed to AFt-TMZ and subsequent generation of
24 γ H2AX foci, support the hypothesis that AFt significantly enhances the delivery of TMZ to
25 cancer cells *in vitro*; overwhelming the direct O6-MeG repair conferred by MGMT. We have
26 additionally encapsulated > 500 molecules of the N3-propargyl imidazotetrazine analog (N3P),
27 developed to combat TMZ resistance, and demonstrated significantly enhanced activity of AFt-
28 N3P against GBM and colorectal carcinoma cell lines. These studies support the use of AFt as
29
30
31
32
33
34
35
36
37
38
39
40
41
42
43
44
45
46
47
48
49
50
51
52
53
54
55
56
57
58
59
60

1
2
3 a promising nano-delivery system for targeted delivery, lysosomal drug release and enhanced
4
5 imidazotetrazine potency for treatment of GBM and wider-spectrum malignancies.
6
7
8
9
10
11
12
13
14
15
16
17
18
19
20
21
22
23
24
25
26
27
28
29
30
31
32
33
34
35
36
37
38
39
40
41
42
43
44
45
46
47
48
49
50
51
52
53
54
55
56
57
58
59
60

1. INTRODUCTION

Glioblastoma multiforme (GBM), a grade (IV) astrocytoma, is the most prevalent and aggressive adult central nervous system (CNS) tumor; presenting heterogeneous, highly angiogenic, invasive and migratory characteristics.¹⁻⁴ GBM cells infiltrate healthy areas of the brain and are thus surrounded by a blood-brain tumor barrier and blood-brain barrier (BBB).⁵ Surgical resection of the tumor followed by radiotherapy coupled with temozolomide (TMZ; **Figure 1a**) chemotherapy confers a median survival rate of ~ 15 months.⁶ Despite the fact that TMZ is able to relatively easily cross the BBB by diffusion, there are concerns associated with poor accumulation of TMZ at the tumor site due to presence of active drug efflux transport proteins such as P-glycoprotein (Pgp) in the BBB and short TMZ plasma half-life ($t_{1/2}$).^{7,8} Indeed, it has been estimated that < 1% of administered drug reaches the brain.⁹ Furthermore, TMZ therapy harbors dose-limiting bone marrow toxicity, hence presenting an additional barrier to successful treatment.¹⁰

Intracellular drug resistance mechanisms further exacerbate efficacy. TMZ is a DNA methylating prodrug. Upon degradation, the active methyldiazonium cation is released and reacts with DNA purine bases, methylating *N3*-adenine, *O6*- and *N7*-guanine.¹¹ *O6*-methylguanine (*O6*-MeG) is the most cytotoxic product produced.^{12,13} The mechanism of action of TMZ has been established¹⁴⁻¹⁶ and it is now accepted that a deficiency in DNA mismatch repair (MMR) leading to *O6*-MeG-thymine mismatch tolerance and overexpression of *O6*-methylguanine-DNA methyltransferase (MGMT), which removes the methyl group from the *O6* position of guanine (restoring normal guanine), are major causes of TMZ resistance *in vitro* and clinically.^{17,18} To overcome TMZ resistance, analogs of TMZ have been developed, whereby *N3*-methyl substitutions with for example *N3*-propargyl (*N3P*), have allowed analogs to evade recognition and removal by MGMT and exert activity independent of DNA mismatch repair (MMR) status.^{19,20}

1
2
3 To enhance brain tumor drug accumulation for greater efficacy and to prevent dose-
4 related toxicity, one approach has been to utilize drug delivery systems (DDS) for targeted drug
5 delivery to tumors.²¹⁻²⁴ Apoferritin (AFt; 480 kDa) is a biocompatible protein cage with an
6 external diameter of 12 nm and internal cavity of 8 nm.^{25,26} The heavy (H) subunits of AFt bind
7 to the transferrin receptor 1 (TfR1),^{27,28} which is overexpressed in cancers (including gliomas)
8 and is also abundantly present on the endothelium of the BBB.^{29,30} Hence, AFt has been
9 proposed as an active drug delivery system for therapeutic agents across the BBB *in vivo*.³¹⁻³³
10 Indeed, there remains an urgent need to develop effective DDS formulations for TMZ and its
11 analogs to enhance efficacy, overcome drug resistance and improve prognoses for patients
12 diagnosed with brain malignancies.
13
14
15
16
17
18
19
20
21
22
23
24
25

26 Herein, we report the encapsulation of TMZ into AFt for GBM-targeted drug delivery,
27 *via* TfR1 uptake. AFt has 14 channels (~ 0.3 – 0.4 nm in diameter) that enable encapsulation
28 of small molecules by diffusion (the so-called ‘nanoreactor’ route). *In vitro* studies have been
29 carried out on the isogenic GBM cancer cell line pair, MGMT-low (U373V) and MGMT-
30 transfected (U373M), together with MMR-deficient and Pgp overexpressing HCT116
31 colorectal carcinoma (CRC) cell lines and non-tumorigenic MRC-5 lung fibroblasts. Enhanced
32 activity of drug within cancerous cells over non-transformed cells upon treatment with
33 encapsulated versus naked drug was demonstrated. Supported by detection of enhanced O6-
34 methylguanine (O6-MeG) adducts and γ H2AX foci in GBM cells exposed to AFt-encapsulated
35 (compared to naked) TMZ, we attribute the observed differential cytotoxicity to AFt-related
36 enhanced delivery, uptake and intracellular retention by cancer cells, allowing release of
37 (intact) TMZ in acidic lysosomes. We additionally demonstrate that further enhancement of
38 activity can be achieved by AFt encapsulation of the TMZ analog bearing the N3P substitution.
39 Our results offer a novel approach for imidazotetrazine formulations that address current
40 limitations, such as drug stability and tumor resistance, associated with TMZ chemotherapy.
41
42
43
44
45
46
47
48
49
50
51
52
53
54
55
56
57
58
59
60

2. MATERIALS AND METHODS

Aft-drug encapsulation: Initially, the reductive demineralization of horse spleen ferritin (Ft; 92% L-subunit: 8% H-subunit) to AFt was carried out.³⁴ TMZ (Sigma-Aldrich) and N3P (synthesized by Helen S. Summers, University of Nottingham) were encapsulated into AFt by diffusion. For both nano-formulations, drug solution in DMSO (10 mM, 7.2 μ moles of TMZ; 6.3 μ moles of N3P) was added to AFt in 0.1 M sodium acetate (NaOAc) buffer (pH 5.5) solution (0.0045 mM, 0.009 μ moles) in small volume increments, every 30 mins (total time 4.5 h), under stirring at 4 °C. The formulations were ultra-filtered using an Amicon ultra-4 centrifugal filter (MWCO: 30 kDa) at 4000 x g for 4 mins and filtered through a 0.22 μ m filter. Samples were stored at 4 °C for further studies.

Nanoparticle characterization: The hydrodynamic size and zeta potential of AFt and nano-formulations diluted in deionized water were measured using Malvern Zetasizer Nano ZS (backscatter angle 173°, λ = 633 nm, T = 25 °C). Samples were filtered (0.22 μ m filter) prior to reading and measured in a disposable DTS1070 cell. Protein size was corroborated *via* red native-PAGE, whereby proteins were stained prior to electrophoresis with Ponceau S (Sigma-Aldrich) to impart negative charge whilst native structure was retained.³⁵ Using a native PAGE 4-16% Bis-Tris pre-cast gel (Invitrogen), samples (1 μ g, 18 μ L) alongside the NativeMark protein standard (Invitrogen, 5 μ L) were resolved at 4 °C, for 1 h at 150 V followed by 1 h at 250 V. Gels were stained with Coomassie brilliant blue G250 for 1 h and left to de-stain overnight in water before imaging with Gene flow limited.

Assessment of encapsulation efficiency and drug loading: Drug concentration in solution was estimated from absorbance measurements using Varian Cary 50 UV-Vis spectrophotometer (λ = 330 nm for TMZ and λ = 328 nm for N3P) with a Suprasil quartz cuvette (Hellma Analytics) and the protein concentration was determined by Bradford assay (see Supplementary Materials, S11).^{36, 37} All measurements were performed in triplicate. For drug release studies, 400 μ L of

1
2
3 Aft nano-formulations were added into a Slide-A-Lyzer 10 kDa MWCO device (Thermo
4 Fisher Scientific) and samples were dialyzed at 37 °C and mixed at 150 rpm against 14 mL of
5
6 either pH 5.5 NaOAc buffer (0.1 M) or pH 7.4 phosphate buffered saline (PBS). After 1, 3, 5,
7
8 7 and 24 h dialysis, drug concentration was measured by UV-Vis spectroscopy. Storage
9
10 stability of Aft formulations at 4 °C, over 7 days, was also monitored for Aft and drug stability
11
12 by using Malvern Zetasizer nano ZS, Bradford assay and UV-Vis spectrophotometer.
13
14

15
16 *Cell culture studies:* Human cell lines used include GBM, U373V (MGMT -) and U373M
17
18 (MGMT +) (gifted by Schering Plough Corporation), colorectal carcinoma (CRC) HCT116
19
20 (MGMT +; hMLH1 -) and HCT116 VR (vincristine resistant; Pgp +)³⁸ and non-tumorigenic
21
22 fetal lung fibroblast, MRC-5 (American Type Tissue Collection (ATCC)) cell lines. GBM cells
23
24 were cultured in RPMI-1640 medium with 10% v/v fetal bovine serum (FBS), 1% v/v non-
25
26 essential amino acids (NEAA), 50 µg/mL gentamicin and 400 µg/mL G418 (Corning).
27
28 HCT116 cells were cultured in RPMI-1640 medium with 10% v/v FBS and MRC-5 cells were
29
30 cultured in minimum essential medium (MEM) with 10% v/v FBS, 1% v/v NEAA, 1% v/v
31
32 penicillin/streptomycin, 2 mM L-glutamine, 10 mM Hepes buffer and 0.075% v/v sodium
33
34 bicarbonate. Cells were maintained in 5% CO₂ at 37 °C. All media and cell culture assay
35
36 components except where otherwise specified were purchased from Sigma-Aldrich.
37
38
39
40

41
42 Growth inhibition of cells was monitored using the 3-(4,5-dimethylthiazol-2-yl)-2,5-
43
44 diphenyltetrazolium bromide (MTT) assay. The MTT assay was performed in 96-well plates
45
46 following 6-day test agent (naked drug, encapsulated drug and naked vehicle) exposure, and at
47
48 the time of treatment at time zero (T0). Seeding densities for GBM cells were 650 cells/well
49
50 and for HCT116 and MRC-5 cells, 400 cells/well. Test agent was introduced into wells (5
51
52 replicates per concentration) 24 h after cell-seeding. MTT reagent (400 µg/ml, Alfa Aesar) was
53
54 added to each well and plates were incubated for 2 h at 37 °C. After 2 h, medium containing
55
56 non-metabolized MTT was aspirated and the insoluble formazan product was dissolved in
57
58
59
60

1
2
3 DMSO (150 μ L). Plates were placed on an orbital shaker for 5 mins and the absorbance was
4
5 measured at $\lambda = 570$ nm with the Perkin Elmer Envision plate reader. At least 3 independent
6
7 repeats for each test agent were performed.
8

9
10 For clonogenic assays, cells were seeded in 6-well plates (400 cells/well) and were exposed to
11
12 TMZ, AFt-TMZ and AFt (50 μ M TMZ; 0.057 μ M AFt) for 24 h and 6 days. Thereafter,
13
14 medium containing test agent was removed, cells were washed with PBS and fresh medium
15
16 was introduced into wells. Plates were incubated at 37 $^{\circ}$ C and the assays terminated when
17
18 colonies of ≥ 50 cells were observed in control wells. Colonies were washed with PBS, fixed
19
20 with 100% methanol, stained with 0.05% methylene blue and counted. Duplicate repeats for
21
22 each test agent were performed in at least 3 independent trials.
23
24

25
26 For live cell counts, GBM cells were seeded in 6-well plates at 1×10^4 cells/well and treated
27
28 with TMZ, AFt-TMZ (TMZ: 50 μ M; AFt: 0.057 μ M) and AFt vehicle (0.057 μ M) for 6 days.
29
30 Then cells were collected by centrifugation (1200 rpm, 5 mins, 4 $^{\circ}$ C). Live cells were counted
31
32 with a hemocytometer using trypan blue (Sigma-Aldrich).
33
34

35
36 Flow cytometry was carried out to examine cell cycle and for γ H2AX foci analysis on GBM
37
38 cells. For cell cycle analysis, cells were seeded in 6-well plates at 1×10^5 cells/well and treated
39
40 with TMZ, AFt-TMZ (TMZ: 50 μ M; AFt: 0.057 μ M) and AFt (0.057 μ M) for 72 h. Cells were
41
42 collected and washed with PBS by centrifugation (1200 rpm, 5 mins, 4 $^{\circ}$ C). Cells were then
43
44 incubated overnight at 4 $^{\circ}$ C, in the dark, with 500 μ L of hypertonic fluorochrome solution
45
46 (0.1% sodium citrate, 0.1% triton X-100, 50 μ g/mL propidium iodide (PI) and 0.1 mg/mL
47
48 ribonuclease A (RNase A) in deionized water). For γ H2AX foci analysis, cells were seeded in
49
50 10 cm tissue culture treated Petri dish at 5×10^5 cells/dish and treated with TMZ, AFt-TMZ
51
52 (TMZ: 50 μ M; AFt: 0.057 μ M and 100 μ M; AFt: 0.1 μ M) and AFt (0.057 and 0.1 μ M) for 48
53
54 and 72 h. Cells were collected and stained using mouse anti-human phospho-histone H2A.X
55
56 (Ser139) primary antibody (1 $^{\circ}$ Ab), clone JBW301 (1:3333; Merck) and F(ab')₂-goat anti-
57
58
59
60

1
2
3 mouse IgG, IgM (H+L) Alexa-Fluor 488 secondary (2°) Ab (1:1750; Invitrogen). The
4
5 fluorescence of 10000 mean gated events (single cells) was obtained using the Beckman
6
7 Coulter FC500 flow cytometer. The data were processed using Weasel v3.0.2 software.

8
9
10 Indirect enzyme-linked immunosorbent assay (ELISA) was carried out for DNA *O6*-MeG
11
12 quantification in GBM cells. Cells were seeded in 6-well plates at $0.1-1 \times 10^5$ cells/well and
13
14 treated with TMZ and Aft-TMZ (50 μ M) for 4, 24, 72 and 144 h. The purification of DNA
15
16 from cells was carried out using the QIAGEN Blood & Cell Culture DNA mini purification
17
18 kits, following the manufacturer's procedure. Double-stranded DNA (1 μ g) was then digested
19
20 with the Timesaver MspI restriction enzyme kit (New England Biolabs), following the
21
22 manufacturer's procedure, and made single-stranded by heating at 95 °C for 10 mins before
23
24 rapidly transferring to ice for at least 15 mins. ELISA was then performed using the IgG (Total)
25
26 Mouse Uncoated ELISA kit (Invitrogen), following the manufacturer's procedure with some
27
28 modifications. Briefly, a 96-well plate was pre-coated with 1% w/v protamine sulfate (Sigma-
29
30 Aldrich) at RT for 1 h, removed and washed 5 times with a jet of milli-Q water. Wells were
31
32 then coated with DNA (10 μ g/mL; 100 μ L) diluted in coating buffer 1x and incubated overnight
33
34 on a shaker at RT. Wells were washed (3x) with eBioscience wash buffer 1x (Invitrogen) and
35
36 blocked with blocking buffer 2x for 2 h, at room temperature (RT). Samples were incubated
37
38 with the 1° monoclonal Ab, mouse anti-human *O6*-MeG (0.2 μ g/mL; Axxora) for 1.5 h at RT,
39
40 followed by incubation with 2° HRP-conjugated anti-mouse IgG polyclonal Ab (1:250) for 1 h
41
42 at RT. Wells were then treated with the tetramethylbenzidine (TMB) substrate solution (100
43
44 μ L) for 15 mins at RT in the dark, quenched with stop solution (100 μ L; Invitrogen) for 5 mins
45
46 at RT and absorbance read at $\lambda = 450$ nm on a Perkin Elmer Envision plate reader. At least 3
47
48 independent repeats for each test agent were performed.

49
50
51 *Western blot:* For protein extraction, cells were collected by centrifugation (1200 rpm, 5 mins,
52
53 4 °C) and lysed in Nonidet-P40 lysis buffer. Protein concentrations were determined by
54
55
56
57
58
59
60

1
2
3 Bradford assay.^{36,37} Protein fractions (50 μ g) were separated by SDS-PAGE (10% resolving
4 gel), transferred onto a nitrocellulose membrane (GE Healthcare Life Sciences) using the
5 Trans-Blot Turbo Transfer System (Bio-Rad) and blocked in 5% skimmed milk in TBST (tris-
6 buffered saline, Tween 20) for 1 h. Membranes were incubated at 4 °C overnight with the
7 following monoclonal 1° Abs, rabbit anti-human TfR1 (1:1000), MGMT (1:1000),
8 glyceraldehyde 3-phosphate dehydrogenase (GAPDH; loading control; 1:1000) (all from Cell
9 Signaling Technology), mouse anti-human Scavenger Receptor Class A Member 5 (SCARA5;
10 1:1000) and transferrin receptor 2 (TfR2; 1:250) (both from R&D systems a bio-technique brand).
11 Membranes were then incubated with 2° Ab (1:4000) for 1 h at RT using either goat anti-rabbit
12 or goat anti-mouse polyclonal antibodies conjugated with horseradish peroxidase (Dako).
13 Bands were visualized on a C-DiGit blot scanner (LI-COR Biosciences) after incubating the
14 membranes with ECL reagent (GE Healthcare) for 5 mins.

15
16
17
18
19
20
21
22
23
24
25
26
27
28
29
30
31 *Imaging cellular morphology:* For environmental scanning electron microscopy (ESEM), a
32 TGS1x0.2 Gold Slot grid (EM Resolutions) was placed at the bottom of a 6-well plate and cells
33 were seeded at 1 x 10⁵ cells/well. After 24 h exposure to TMZ and AFt-TMZ (50 μ M), cells
34 were fixed with 3.7% v/v formaldehyde in PBS for 5 mins. The grids were washed and stored
35 in PBS. Immediately prior to imaging, grids were rinsed with deionized water and mounted on
36 a stage set at 3 °C. The chamber pressure was dropped to 5.15 Torr, with humidity set to 87 %.
37 Images were acquired using FEI Quanta 650 ESEM operating using a 5 kV electron beam and
38 magnification x1000. For confocal microscopy, GBM cells were seeded in an 8-well μ -slide
39 plate (Ibidi) at 1 x 10⁴ cells/well and treated for 24 h with TMZ and AFt-TMZ (50 μ M).
40 Following treatment, cells were washed with PBS, fixed with 3.7% v/v formaldehyde (15 mins)
41 and permeabilized with 0.1% v/v triton X-100. Cells were then co-stained for 1 h with F-actin
42 phalloidin-iFluor 633 (1x) and nuclear DAPI (0.02 μ g/ml) stains. Wells were washed twice
43 with PBS before storing in PBS (200 μ L) for imaging. Imaging was performed with a 63x water
44
45
46
47
48
49
50
51
52
53
54
55
56
57
58
59
60

1
2
3 magnification lens using Zeiss Elyra PS1 super resolution microscope with DAPI excitation at
4 405 nm and phalloidin excitation at 633 nm. Confocal images were analyzed using the Fiji
5 Image J software.
6
7

8
9
10 *Statistical analysis.* Two-way or three-way ANOVA analysis function on GraphPad Prism
11 version 8.2.1 was used to determine the differences between multiple groups ($n \geq 3$). Values of
12 *P or #P < 0.05, **P or ##P < 0.01, ***P or ###P < 0.001 and ****P or ####P < 0.0001 were
13 considered as statistically significant. Data are represented as the means \pm SD.
14
15
16
17
18
19
20
21
22

23 3. RESULTS AND DISCUSSION

24
25
26 The AFt protein cage has an external diameter \sim 12 nm suitable for passive targeting *via* the
27 enhanced permeability and retention (EPR) effect.³⁹ TfR1 binding sites on the H-polypeptide
28 subunits of AFt allow active targeting of AFt-encapsulated cargo. TfR1 has been shown to be
29 overexpressed by GBM (but not glial) and present on BBB endothelial cells, but not peripheral
30 endothelium.³⁰ TfR1 has been shown to be an important receptor for cancers due to their
31 increased iron demand.⁴⁰ We hence evaluated the loading of TMZ into AFt for GBM targeting,
32 with the goal to achieve enhanced transport of the molecules across the BBB, delivery to, and
33 accumulation within cancer cells. AFt-encapsulation of TMZ may also minimize premature
34 degradation and elimination, efflux (mediated by Pgp) and drug-related side effects. The small
35 size of the test agent (< 300 g/mol) allows its encapsulation *via* the ‘nanoreactor’ route, where
36 passive diffusion across the 0.3 - 0.4 nm channels is feasible.^{37,41,42} Briefly, test agent was
37 added gradually over 4.5 h to AFt at pH 5.5 to permit encapsulation under diffusion to take
38 place (**Figure 1b**) and to avoid TMZ degradation, which occurs at physiological pH \sim 7.4 (*in*
39 *vitro* $t_{1/2}$ of TMZ at pH 7.4 is 1.9 h;⁸ at pH 5.5 $t_{1/2} > 100$ h). We achieved $84.3 \pm 5.2\%$
40 encapsulation efficiency (EE) and $18.7 \pm 2.3\%$ drug loading (DL), which corresponds to \sim 520
41
42
43
44
45
46
47
48
49
50
51
52
53
54
55
56
57
58
59
60

1
2
3 drug molecules per AFt cage (see also Supplementary Information, S11). The integrity of the
4
5 AFt cage following drug encapsulation and absence of drug attachment to the AFt exterior was
6
7 confirmed by DLS and zeta potential measurements; no noticeable change in either
8
9 hydrodynamic size or zeta potential was observed, with average hydrodynamic diameter of
10
11 13.3 ± 0.9 nm and zeta potential of -12.7 ± 0.3 mV for AFt before and after TMZ encapsulation
12
13 (**Figure 1c**). Native PAGE of AFt-TMZ revealed protein bands at molecular weight (MW) ~
14
15 480 and 720 kDa (dimer), comparable to those of AFt alone (**Figure 1d**), confirming successful
16
17 encapsulation of the agents inside the AFt cavity. By optimizing the encapsulation conditions
18
19 and performing step-wise addition of the drug, we achieved improved drug loading (~ 520
20
21 molecules per AFt cage) compared to previously reported values of up to 100 – 350 molecules
22
23 of GW608 and its derivatives and 185 molecules of triazene, 5-(3-methyltriazene-1-yl)
24
25 imidazole-4-carboxamide (MTIC).^{37,43} We attribute enhanced DL, to the small molecular
26
27 weight and good solubility profiles of TMZ.
28
29
30
31
32

33 We assessed the release of drugs from AFt under physiologically relevant conditions
34
35 ($T = 37$ °C, pH 7.4 and pH 5.5; see Supplementary Information S11, Figure S2) and observed
36
37 slower drug release within the first 3 h at pH 7.4 compared to pH 5.5. This observation is
38
39 consistent with the expectation that AFt channels are narrower at more alkali pH and gradually
40
41 widen as the capsule relaxes with increasing acidity.⁴⁴ The storage stability of the AFt
42
43 formulation (at $T = 4$ °C) was monitored and no apparent change in protein size, zeta potential
44
45 or drug:AFt ratio were observed over a period of at least 7 days (Supplementary Information
46
47 S11, Figure S3).
48
49
50

51 The *in vitro* anti-cancer activity of TMZ delivered by AFt was subsequently evaluated.
52
53 Initially, MTT assays were employed and the following cell lines utilized for our studies:
54
55 U373V (MGMT -), U373M (MGMT +) GBM; HCT116 (MMR deficient), HCT116 VR (Pgp
56
57 +) CRC and non-cancerous MRC-5 fibroblasts. The growth inhibitory activity of AFt-TMZ
58
59
60

1
2
3 was compared to unencapsulated (naked) TMZ. The cells were exposed to test agent with
4 concentrations ranging from 0.001 - 1000 μM . Cellular growth inhibition (estimated GI_{50}
5 values) was determined (**Figure 2**). Cells were exposed to test agents for 6 days, allowing
6 enough time for a minimum of 2 cell cycle rounds, DNA methylation and MMR activation.
7
8 Aft-TMZ demonstrated markedly enhanced activity over naked TMZ. GI_{50} values of 35 μM
9 and 376 μM were calculated for TMZ in U373V and U373M cells respectively. Remarkably,
10 Aft-TMZ demonstrated significantly lower GI_{50} values (enhanced activity) of $< 1.5 \mu\text{M}$ in both
11 U373V and U373M cell lines. Of interest, and contrary to expectations, Aft-encapsulated TMZ
12 displayed enhanced activity over naked TMZ in cell lines that showed resistance to TMZ,
13 where resistance was conferred by MGMT (532-fold enhanced activity in U373M), MMR loss
14 (22-fold in HCT116) and additionally Pgp expression (24-fold in HCT116 VR).
15
16
17
18
19
20
21
22
23
24
25
26
27
28

29 Cancer-selective activity was also seen, with Aft-TMZ demonstrating enhanced
30 activity against cancer cells over fibroblasts by ~ 5 -fold. Alone, Aft did not display growth
31 inhibitory activity against any of the cell lines at concentrations $\leq 1 \mu\text{M}$ (equivalent to the
32 highest concentration of Aft in Aft-drug used in the assay). In support of this study, live cell
33 count assays (Supplementary Information, SI2) demonstrated greater significant loss of viable
34 cells with Aft-TMZ treatment against U373M compared to naked TMZ ($P < 0.0001$).
35
36 Interestingly, Fang *et al.* demonstrated that conjugation of TMZ to chitosan nanoparticles could
37 partially overcome TMZ-resistance.²³ Kumari *et al.* also reported this phenomenon with TMZ-
38 loaded lactoferrin nanoparticles.²⁴ Recently reported is the Aft-encapsulation of the combined
39 TMZ-intermediate, MTIC, with copper.⁴³ We postulate that the enhanced activity of TMZ
40 encapsulated within Aft is due to a different mode of cellular uptake (*via* TfR1 recognition).
41
42 Aft rapidly enters and accumulates inside lysosomes following TfR1 receptor mediated
43 endocytosis,²⁷ therefore evasion of Pgp efflux may be possible. Consequently, enhanced
44 intracellular accumulation of TMZ results in greater potency.
45
46
47
48
49
50
51
52
53
54
55
56
57
58
59
60

1
2
3 In order to test this hypothesis, we examined cellular expression of proteins responsible
4 for AFt uptake and resistance to TMZ. Protein lysates prepared from the cancer cells used in
5 this study revealed TfR1 expression whereas in MRC-5 lysates, expression was below the limit
6 of detection (**Figure 3** and supplementary Figure S5). Since the expression of SCARA5 and
7 TfR2 was not observed, we conclude that TfR1 is the receptor responsible for AFt uptake,
8 providing some selective anti-cancer activity for our formulation. Western blot also confirmed
9 the presence of MGMT, which confers TMZ resistance, in U373M and its absence in U373V.

10
11
12 To substantiate the results of AFt-TMZ activity against TMZ-resistant U373M,
13 clonogenic assays were employed. **Figure 4** illustrates the survival fraction of U373V and
14 U373M colonies after 24 h and 6 days exposure to naked and encapsulated TMZ (see also
15 Supplementary Information SI2). AFt alone had negligible effect on colony numbers
16 confirming the biocompatibility of this drug delivery vehicle, however, AFt-encapsulation of
17 TMZ augmented the drug's inhibition of colony formation in both U373V and U373M GBM
18 cells. TMZ alone (50 μ M) potently inhibited U373V colony formation by 68% and 84% after
19 24 h and 6 d exposure, respectively; whereas, U373M cells demonstrated much greater
20 resistance to naked TMZ challenge (colony formation inhibited by 14% and by 35% after 24 h
21 and 6 d exposure, respectively). In contrast, 24 h and 6 d AFt-TMZ exposure potently inhibited
22 U373M colony formation by 47% and 76% respectively. U373M cells were significantly less
23 able to survive AFt-TMZ challenge (compared to naked TMZ) and form progeny colonies;
24 AFt-TMZ displayed 2.7-fold enhanced toxicity compared to naked TMZ, supporting MTT
25 assays and cell counts further demonstrating that AFt-delivery of TMZ is able to weaken tumor
26 resistance to TMZ mediated by MGMT.

27
28
29 Following the assessment of AFt-TMZ cytotoxicity, GBM cell cycle progression was
30 probed after 72 h exposure of cells to TMZ and AFt-TMZ. Treatment periods of 72 h were
31 adopted to allow cells to complete at least one division for detection of putative cell cycle
32
33
34
35
36
37
38
39
40
41
42
43
44
45
46
47
48
49
50
51
52
53
54
55
56
57
58
59
60

1
2
3 perturbation by AFt-TMZ. It is known that TMZ (in the absence of MGMT) alkylates DNA
4 causing S and G2/M arrest.^{13,14} G2/M arrest can be seen following treatment with TMZ in
5 U373V cells only; however, both U373V and U373M cells expressed greater G2/M- and S-
6 phase arrest following exposure to AFt-TMZ (**Figure 5a**, and Supplementary Information,
7 SI2). Compared to U373V control populations, S-phase arrest was increased by ~ 2.5- and 2.6-
8 fold with TMZ and AFt-TMZ, respectively; G2/M-phase arrest was increased by ~ 2.3- and
9 2.8-fold, respectively. As for U373M, S- and G2/M-phase arrest was increased by 1.87- and 2-
10 fold, respectively, following treatment with AFt-TMZ. TMZ alone failed to significantly
11 perturb U373M cell cycle progression. Cell cycle profiles indistinguishable from controls were
12 observed following exposure of cells to AFt alone. Assessment of *O6*-MeG levels in the DNA
13 of cells following treatment with TMZ and AFt-TMZ (4 – 144 h), revealed that AFt-TMZ
14 delivered significantly more ($P < 0.001$) methyl groups to *O6*-guanine than TMZ alone (**Figure**
15 **5b**).

16
17
18
19
20
21
22
23
24
25
26
27
28
29
30
31
32
33 Since AFt-TMZ was shown to transcend the resistance systems in GBM cells, evoking
34 significantly enhanced activity over TMZ alone, we sought to establish whether the increased
35 *O6*-MeG levels and S- and G2/M-phase arrest translated to greater DNA damage following
36 treatment for 48 and 72 h. The presence of γ H2AX foci is indicative of DNA double strand
37 breaks and as such, our studies have demonstrated that greater levels of γ H2AX foci were
38 observed following treatment of U373V and U373M cells with AFt-TMZ (compared to TMZ
39 alone; **Figure 5c**). These levels were shown to increase in both a time- and concentration-
40 dependent manner. In U373V and U373M, 72 h exposure to 50 μ M AFt-TMZ yielded
41 respectively 1.2- and 1.4-fold significantly more DNA double strand breaks over TMZ alone
42 ($P < 0.001$). This corroborated well with the trends observed in cell cycle and *O6*-MeG
43 analyses.
44
45
46
47
48
49
50
51
52
53
54
55
56
57
58
59
60

1
2
3 We further evaluated the effect of AFt-TMZ treatment on GBM cells using ESEM in
4 order to observe changes to the cell surface after brief exposure of cells to test agents. It was
5 apparent that the spread of the cells was greatly affected by AFt-TMZ, more so than by naked
6 TMZ after 24 h treatment exposure (**Figure 6**). In contrast to the control cells, those treated
7 with AFt-TMZ appeared more shrunken, with blebs apparent on their surfaces; being most
8 obvious on U373M. Confocal microscopy studies carried out on stained actin filaments using
9 phalloidin further corroborated the ESEM work. The intensity of the phalloidin stain was at its
10 lowest with AFt-TMZ; a more shrunken cellular morphology most likely indicates reduced
11 uptake of F-actin stain (Supplementary Information, SI2, Figure S9). Cell shrinkage and
12 blebbing may signify apoptosis. F-actin cytoskeleton is an essential component in regulation
13 of cell shape, migration and division and its reduction infers loss of these capabilities.⁴⁵ These
14 methodologies have demonstrated that AFt-TMZ affects cellular morphology as early as 24 h
15 post treatment.

16
17
18
19
20
21
22
23
24
25
26
27
28
29
30
31
32
33 The promising, enhanced anti-cancer activity achieved with AFt-TMZ encouraged us
34 to pursue AFt-encapsulation of N3P, an analog of TMZ where N3-methyl has been replaced
35 with a propargyl moiety (**Figure 7**). N3P was designed to deliver propargyl lesions onto
36 susceptible DNA bases that cannot be removed by MGMT. Indeed, TAQ polymerase assays
37 demonstrated alkylation at runs of guanine – akin to those caused by TMZ, and anti-tumor
38 activity was seen irrespective of MGMT or MMR status.^{19,20} However, N3P possesses inferior
39 (in comparison to TMZ) pharmacokinetic properties ($t_{1/2} = 49$ min at pH 7.4), potentially
40 thwarting efficient delivery to the brain and therapeutic utility. Like TMZ, N3P is acid-stable
41 ($t_{1/2} > 100$ h at pH 5.5), therefore, N3P was encapsulated within AFt cages using the same
42 diffusion method optimized for TMZ. Similar loading efficiency of ~ 525 molecules per AFt
43 capsule was achieved ($EE = 70.5 \pm 3.3\%$ and $DL = 20.5 \pm 3.1\%$). No noticeable change in
44 hydrodynamic size and zeta potential was observed, with average hydrodynamic diameter of
45
46
47
48
49
50
51
52
53
54
55
56
57
58
59
60

1
2
3 13.1 ± 0.7 nm and zeta potential of -12.5 ± 0.4 mV for AFt before and after N3P encapsulation
4 (Figure 7a). Native PAGE of AFt-N3P revealed protein bands at MW ~ 480 and 720 kDa,
5
6 comparable to those of AFt alone; confirming successful encapsulation of the agent inside the
7
8 AFt cavity. *In vitro* growth inhibitory studies on GBM cell lines, U373V (MGMT –) and
9
10 U373M (MGMT +), HCT 116 (MMR deficient) and non-cancerous MRC-5 fibroblasts (Figure
11
12 7b) demonstrated enhanced activity with lower GI₅₀ values compared to TMZ in both GBM
13
14 cell lines: GI₅₀ value of < 0.25 μM for AFt-N3P. The AFt-N3P formulation retained a degree
15
16 of selectivity, with ~ 9-fold greater activity in cancer cells compared to fibroblasts.
17
18
19
20
21

22 Therefore, development of AFt-formulations of TMZ and N3P represents a promising
23
24 strategy to challenge TMZ resistance in malignant brain tumors such as GBM, and wider
25
26 spectrum cancer phenotypes. Furthermore, the surface of AFt can be modified with additional
27
28 surface ligands (e.g. GKRK peptides) for enhanced tumor accumulation *in vivo* and BBB
29
30 penetrance.^{31,46} Preclinical effects of AFt delivery of imidazotetrazine molecules will be further
31
32 evaluated *in vivo*.
33
34
35
36
37

38 4. CONCLUSIONS

39
40
41 In conclusion, we have successfully loaded > 500 molecules of TMZ and N3P per AFt cage,
42
43 *via* the nanoreactor route, achieving EE > 70% and DL > 18%, and maintaining AFt capsule
44
45 integrity. *In vitro* studies demonstrated that both AFt nano-formulations displayed significantly
46
47 enhanced activity over naked drugs against MGMT +/- GBM cell lines. Most intriguingly, this
48
49 includes AFt-TMZ, which *in vitro* overcame tumor resistance mediated by MGMT.
50
51 Accumulation of O6-MeG adducts, cell cycle arrest and subsequent generation of γH2AX in
52
53 U373M support the hypothesis that TfR1, expressed by cancer cell lines used in this study,
54
55 mediates increased intracellular accumulation of TMZ that is able to overwhelm the suicide
56
57 repair protein MGMT and confer sensitivity to TMZ in MGMT + GBM cells. If O6-guanine
58
59
60

1
2
3 methylation outpaces MGMT protein synthesis, its depletion would ensue ⁴⁷ – as is indicated
4 following exposure of U373M cells to AFt-TMZ (Bouzinab unpublished results). Moreover,
5
6 evidence suggests other mechanisms conferring tolerance or resistance to TMZ may be
7
8 weakened (including MMR-deficiency and Pgp expression) following its encapsulation in AFt.
9
10 In addition, AFt encapsulation of imidazotetrazine analog N3P resulted in enhanced anti-tumor
11
12 activity and cancer cell line-selectivity. Importantly, AFt alone was non-toxic. These findings
13
14 lay the foundations for AFt, a biocompatible, species-specific nanosized biomaterial with built
15
16 in targeting, to deliver concentrated amounts of anti-cancer small molecules to tumors.
17
18
19
20
21
22
23
24
25
26
27
28
29
30
31
32
33
34
35
36
37
38
39
40
41
42
43
44
45
46
47
48
49
50
51
52
53
54
55
56
57
58
59
60

1
2
3 ASSOCIATED CONTENT
4
5

6 **Supporting Information.** Supporting information included methodology and
7
8 characterization data. The following file is available: Supporting Information.pdf
9
10

11
12 AUTHOR INFORMATION
13

14
15 **Corresponding Authors**
16

17 * Dr Lyudmila Turyanska Lyudmila.Turyanska@nottingham.ac.uk
18

19 Dr Tracey D Bradshaw Tracey.Bradshaw@nottingham.ac.uk
20

21 University of Nottingham, NG7 2RD Nottingham, UK
22
23

24
25 **Author Contributions**
26

27 The manuscript was written through contributions of all authors. All authors have given
28
29 approval to the final version of the manuscript.
30
31

32
33 **Funding Sources**
34

35 Engineering and Physical Sciences Research Council [grant number EP/L01646X/1 and
36
37 EP/L022494/1].
38
39

40
41 CONFLICTS OF INTEREST
42

43
44 The authors declare no conflicts of interest and no competing financial interest.
45
46
47
48

49
50 ACKNOWLEDGMENTS
51

52 This work was funded by the Engineering and Physical Sciences Research Council [grant
53
54 number EP/L01646X/1; EP/L022494/1; EP/P03/1684/1] and the EPSRC Centre for Doctoral
55
56 Training in Advanced Therapeutics and Nanomedicines; University of Nottingham and
57
58 AstraZeneca. The authors acknowledge the Nanoscale and Microscale Research Centre
59
60

1
2
3 (nmRC) for providing access to instrumentation and to Dr. David Onions and Dr. Robert
4
5 Markus for useful discussions and technical support. Authors acknowledge support from
6
7 Children with Cancer UK and Josephine R. Poole for cover art.
8
9
10
11
12
13
14
15
16
17
18
19
20
21
22
23
24
25
26
27
28
29
30
31
32
33
34
35
36
37
38
39
40
41
42
43
44
45
46
47
48
49
50
51
52
53
54
55
56
57
58
59
60

REFERENCES

- (1) Parsons, D.; Jones, S.; Zhang, X.; Lin, J.; Leary, R.; Angenendt, P.; Mankoo, P.; Carter, H.; Siu, I. M.; Gallia, G. L.; Olivi, A.; McLendon, R.; Rasheed, B. A.; Keir, S.; Nikolskaya, T.; Nikolsky, Y.; Busam, D. A.; Tekleab, H.; Diaz, L. A., Jr.; Hartigan, J.; Smith, D. R.; Strausberg, R. L.; Marie, S. K.; Shinjo, S. M.; Yan, H.; Riggins, G. J.; Bigner, D. D.; Karchin, R.; Papadopoulos, N.; Parmigiani, G.; Vogelstein, B.; Velculescu, V. E.; Kinzler, K. W. An Integrated Genomic Analysis of Human Glioblastoma Multiforme. *Science* **2008**, *321*, 1807-1812.
- (2) Phillips, H. S.; Kharbanda, S.; Chen, R.; Forrest, W. F.; Soriano, R. H.; Wu, T. D.; Misra, A.; Nigro, J. M.; Colman, H.; Soroceanu, L.; Williams, P. M.; Modrusan, Z.; Feuerstein, B. G.; Aldape, K. Molecular subclasses of high-grade glioma predict prognosis, delineate a pattern of disease progression, and resemble stages in neurogenesis. *Cancer Cell* **2006**, *9*, 157-173.
- (3) Beroukhi, R.; Getz, G.; Nghiemphu, L.; Barretina, J.; Hsueh, T.; Linhart, D.; Vivanco, I.; Lee, J. C.; Huang, J. H.; Alexander, S.; Du, J.; Kau, T.; Thomas, R. K.; Shah, K.; Soto, H.; Perner, S.; Prensner, J.; Debiasi, R. M.; Demichelis, F.; Hatton, C.; Rubin, M. A.; Garraway, L. A.; Nelson, S. F.; Liao, L.; Mischel, P. S.; Cloughesy, T. F.; Meyerson, M.; Golub, T. A.; Lander, E. S.; Mellinghoff, I. K.; Sellers, W. R. Assessing the significance of chromosomal aberrations in cancer: Methodology and application to glioma. *Proc. Natl. Acad. Sci. U.S.A.* **2007**, *104*, 20007-20012.
- (4) Smith, C. L.; Kilic, O.; Schiapparelli, P.; Guerrero-Cazares, H.; Kim, D. H.; Sedora-Roman, N. I.; Gupta, S.; O'Donnell, T.; Chaichana, K. L.; Rodriguez, F. J.; Abbadi, S.; Park, J.; Quiñones-Hinojosa, A.; Levchenko, A. Migration Phenotype of Brain-Cancer Cells Predicts Patient Outcomes. *Cell Rep.* **2016**, *15*, 2616-2624.
- (5) Watkins, S.; Robel, S.; Kimbrough, I. F.; Robert, S. M.; Ellis-Davies, G.; Sontheimer, H. Disruption of astrocyte–vascular coupling and the blood–brain barrier by invading glioma cells. *Nat. Commun.* **2014**, *5*, 4196.
- (6) Brodbelt, A.; Greenberg, D.; Winters, T.; Williams, M.; Vernon, S.; Collins, V. P. Glioblastoma in England: 2007–2011. *Eur. J. Cancer* **2015**, *51*, 533-542.
- (7) de Gooijer, M. C.; de Vries, N. A.; Buckle, T.; Buil, L. C. M.; Beijnen, J. H.; Boogerd, W.; van Tellingen, O. Improved Brain Penetration and Antitumor Efficacy of Temozolomide by Inhibition of ABCB1 and ABCG2. *Neoplasia* **2018**, *20*, 710-720.
- (8) Baker, S. D.; Wirth, M.; Statkevich, P.; Reidenberg, P.; Alton, K.; Sartorius, S. E.; Dugan, M.; Cutler, D.; Batra, V.; Grochow, L. B.; Donehower, R. C.; Rowinsky, E. K. Absorption, metabolism, and excretion of ¹⁴C-temozolomide following oral administration to patients with advanced cancer. *Clin. Cancer Res.* **1999**, *5*, 309-17.
- (9) Groothuis, D. R. The blood-brain and blood-tumor barriers: A review of strategies for increasing drug delivery. *Neuro-Oncology* **2000**, *2*, 45-59.
- (10) Newton, S.; Kalamaha, K.; Fernandes, H. Temozolomide-induced Aplastic Anemia Treated with Eltrombopag and Granulocyte Colony Stimulating Factor: A Report of a Rare Complication. *Cureus* **2018**, *10*, e3329.

- 1
2
3 (11) Zhang, J.; Stevens, M. F.; Bradshaw, T. D. Temozolomide: Mechanisms of Action, Repair
4 and Resistance. *Curr. Mol. Pharmacol.* **2012**, *5*, 102-114.
5
6 (12) Denny, B. J.; Wheelhouse, R. T.; Stevens, M. F.; Tsang, L. L. Slack, J. A. NMR and
7 Molecular Modeling Investigation of the Mechanism of Activation of the Antitumor Drug
8 Temozolomide and Its Interaction with DNA. *Biochemistry* **1994**, *33*, 9045-9051.
9
10 (13) Tisdale M. J. Antitumour imidazotetrazines—XV: Role of guanine O⁶ alkylation in the
11 mechanism of cytotoxicity of imidazotetrazinones. *Biochem. Pharmacol.* **1987**, *36*, 457-462.
12
13 (14) Mojas, N.; Lopes, M.; Jiricny, J. Mismatch repair-dependent processing of methylation
14 damage gives rise to persistent single-stranded gaps in newly replicated DNA. *Genes Dev.*
15 **2007**, *21*, 3342-3355.
16
17 (15) He, Y.; Kaina, B. Are There Thresholds in Glioblastoma Cell Death Responses Triggered
18 by Temozolomide? *Int. J. Mol. Sci.* **2019**, *20*, 1562.
19
20 (16) Roos, W.; Baumgartner, M.; Kaina, B. Apoptosis triggered by DNA damage O⁶-
21 methylguanine in human lymphocytes requires DNA replication and is mediated by p53 and
22 Fas/CD95/Apo-1. *Oncogene* **2004**, *23*, 359-367.
23
24 (17) Cejka, P.; Stojic, L.; Mojas, N.; Russell, A. M.; Heinemann, K.; Cannavó, E.; di Pietro,
25 M.; Marra, G.; Jiricny, J. Methylation-induced G2/M arrest requires a full complement of the
26 mismatch repair protein hMLH1. *EMBO J.* **2003**, *22*, 2245-2254.
27
28 (18) Kitange, G. J.; Carlson, B. L.; Schroeder, M. A.; Grogan, P. T.; Lamont, J. D.; Decker, P.
29 A.; Wu, W.; James, C. D.; Sarkaria, J. N. Induction of MGMT expression is associated with
30 temozolomide resistance in glioblastoma xenografts. *Neuro-Oncology* **2009**, *11*, 281-291.
31
32 (19) Zhang, J.; Hummersone, M. G.; Matthews, C. S.; Stevens, M. F. Bradshaw, T. D. N3-
33 Substituted Temozolomide Analogs Overcome Methylguanine-DNA Methyltransferase and
34 Mismatch Repair Precipitating Apoptotic and Autophagic Cancer Cell Death. *Oncology* **2015**,
35 *88*, 28-48.
36
37 (20) Cousin, D.; Zhang, J.; Hummersone, M. G.; Matthews, C. S.; Frigerio, M.; Bradshaw, T.
38 D.; Stevens, M. F. Antitumor imidazo[5,1-d]-1,2,3,5-tetrazines: compounds modified at the 3-
39 position overcome resistance in human glioblastoma cell lines. *Med. Chem. Commun.* **2016**, *7*,
40 2332-2343.
41
42 (21) Kim, J.; Ahn, S. I.; Kim, Y. Nanotherapeutics engineered to cross the blood-brain barrier
43 for advanced drug delivery to the central nervous system. *J. Ind. Eng. Chem.* **2019**, *73*, 8-18.
44
45 (22) Oberoi, R. K.; Parrish, K. E.; Sio, T. T.; Mittapalli, R. K.; Elmquist, W. F.; Sarkaria, J. N.
46 Strategies to improve delivery of anticancer drugs across the blood-brain barrier to treat
47 glioblastoma. *Neuro-Oncology* **2015**, *18*, 27-36.
48
49 (23) Fang, C.; Wang, K.; Stephen, Z. R.; Mu, Q.; Kievit, F. M.; Chiu, D. T.; Press, O. W.;
50 Zhang, M. Temozolomide Nanoparticles for Targeted Glioblastoma Therapy. *ACS Appl.*
51 *Mater. Interfaces* **2015**, *7*, 6674-6682.
52
53
54
55
56
57
58
59
60

- 1
2
3 (24) Kumari, S.; Ahsan, S. M.; Kumar, J. M.; Kondapi, A. K.; Rao, N. M. Overcoming blood
4 brain barrier with a dual purpose Temozolomide loaded Lactoferrin nanoparticles for
5 combating glioma (SERP-17-12433). *Sci. Rep.* **2017**, *7*, 6602.
6
7 (25) Ford, G. C.; Harrison, P. M.; Rice, D. W.; Smith, J. M.; Treffry, A.; White, J. L.; Yariv,
8 J. Ferritin: Design and Formation of an Iron-Storage Molecule. *Philos. Trans. R. Soc., B* **1984**,
9 *304*, 551-565.
10
11 (26) Crichton, R. R.; Bryce, C. F. Subunit interactions in horse spleen apoferritin. Dissociation
12 by extremes of pH. *Biochem. J.* **1973**, *133*, 289-299.
13
14 (27) Li, L.; Fang, C. J.; Ryan, J. C.; Niemi, E. C.; Lebrón, J. A.; Björkman, P. J.; Arase, H.;
15 Torti, F. M.; Torti, S. V.; Nakamura, M. C.; Seaman, W. E. Binding and uptake of H-ferritin
16 are mediated by human transferrin receptor-1. *Proc. Natl. Acad. Sci. U.S.A.* **2010**, *107*, 3505-
17 3510.
18
19 (28) Zhang, L.; Li, L.; Di Penta, A.; Carmona, U.; Yang, F.; Schöps, R.; Brandsch, M.; Zugaza,
20 J. L.; Knez, M. H-Chain Ferritin: A Natural Nuclei Targeting and Bioactive Delivery
21 Nanovector. *Adv. Healthcare Mater.* **2015**, *4*, 1305–1310.
22
23 (29) Jefferies, W. A.; Brandon, M. R.; Hunt, S. V.; Williams, A. F.; Gatter, K. C.; Mason, D.
24 Y. Transferrin receptor on endothelium of brain capillaries. *Nature* **1984**, *312*, 162-163.
25
26 (30) Johnsen, K. B.; Burkhart, A.; Melander, F.; Kempen, P. J.; Vejlebo, J. B.; Siupka, P.;
27 Nielsen, M. S.; Andresen, T. L.; Moos, T. Targeting transferrin receptors at the blood-brain
28 barrier improves the uptake of immunoliposomes and subsequent cargo transport into the brain
29 parenchyma. *Sci. Rep.* **2017**, *7*, 10396.
30
31 (31) Zhai, M.; Wang, Y.; Zhang, L.; Liang, M.; Fu, S.; Cui, L.; Yang, M.; Gong, W.; Li, Z.;
32 Yu, L.; Xie, X.; Yang, C.; Yang, Y.; Gao, C. Glioma targeting peptide modified apoferritin
33 nanocage. *Drug Delivery* **2018**, *25*, 1013-1024.
34
35 (32) Chiou, B.; Connor, J. R. Emerging and dynamic biomedical uses of ferritin.
36 *Pharmaceuticals* **2018**, *11*, E124.
37
38 (33) Macone, A.; Masciarelli, S.; Palombarini, F.; Quaglio, D.; Boffi, A.; Trabuco, M. C.;
39 Baocco, P.; Fazi, F.; Bonamore, A. Ferritin nanovehicle for targeted delivery of cytochrome C
40 to cancer cells. *Sci. Rep.* **2019**, *9*, 11749.
41
42 (34) Wong, K. K.; Cölfen, H.; Whilton, N. T.; Douglas, T.; Mann, S. Synthesis and
43 characterization of hydrophobic ferritin proteins. *J. Inorg. Biochem.* **1999**, *76*, 187-195.
44
45 (35) Dráb, T.; Kračmerová, J.; Tichá, I.; Hanzlíková, E.; Tichá, M.; Ryšlavá, H.; Doubnerová,
46 V.; Maňásková-Postlerová, P.; Liberda, J. Native Red Electrophoresis – A new method suitable
47 for separation of native proteins. *Electrophoresis* **2011**, *32*, 3597-3599.
48
49 (36) Bradford, M. M. A rapid and sensitive method for the quantitation of microgram quantities
50 of protein utilizing the principle of protein-dye binding. *Anal. Biochem.* **1976**, *72*, 248-254.
51
52 (37) Breen, A. F.; Wells, G.; Turyanska, L.; Bradshaw, T. D. Development of novel apoferritin
53 formulations for antitumour benzothiazoles. *Cancer Reports* **2019**, *2*, e1155.
54
55
56
57
58
59
60

- 1
2
3 (38) Qazzaz, M. E.; Raja, V. J.; Lim, K. H.; Kam, T. S.; Lee, J. B.; Gershkovich, P.; Bradshaw,
4 T. D. *In vitro* anticancer properties and biological evaluation of novel natural alkaloid
5 jerantinine b. *Cancer Lett.* **2016**, *370*, 185-197.
6
7 (39) Grobmyer, S. R.; Moudgil, B. M. In *Cancer nanotechnology: methods and protocols;*
8 *Methods in molecular biology (Clifton, N.J.)*, Vol. 624; Springer protocols; Humana Press:
9 New York, 2010.
10
11 (40) Torti, S. V.; Torti, F. M. Iron and cancer: more ore to be mined. *Nat. Rev. Cancer* **2013**,
12 *13*, 342-355.
13
14 (41) Bouzinab, K.; Summers, H.; Zhang, J.; Stevens, M. F. G.; Moody, C. J.; Turyanska, L.;
15 Thomas, N. R.; Gershkovich, P.; Ashford, M. B.; Vitterso, E.; Storer, L. C D.; Grundy, R.;
16 Bradshaw, T. D. In search of effective therapies to overcome resistance to temozolomide in
17 brain tumours. *Cancer Drug Resist.* **2019**, *2*, 1018-1031.
18
19 (42) Kuruppu, A. I.; Zhang, L.; Collins, H.; Turyanska, L.; Thomas, N. R.; Bradshaw, T. D.
20 An apoferritin-based drug delivery system for the Tyrosine Kinase Inhibitor Gefitinib. *Adv.*
21 *Healthcare Mater.* **2015**, *4*, 2816-2821.
22
23 (43) Li, X.; Shao, F.; Sun, J.; Du, K.; Sun, Y.; Feng, F. Enhanced copper–temozolomide
24 interactions by protein for chemotherapy against glioblastoma multiforme. *ACS Appl. Mater.*
25 *Interfaces* **2019**, *11*, 41935-41945.
26
27 (44) Kim, M.; Rho, Y.; Jin, K. S.; Ahn, B.; Jung, S.; Kim, H.; Ree, M. pH-Dependent Structures
28 of Ferritin and Apoferritin in Solution: disassembly and reassembly. *Biomacromolecules* **2011**,
29 *12*, 1629-1640.
30
31 (45) Stricker, J.; Falzone, T.; Gardel, M. Mechanics of the F-actin Cytoskeleton. *J Biomech.*
32 **2010**, *43*, 9-20.
33
34 (46) Al-Ani, A. W.; Zhang, L.; Ferreira, L.; Turyanska, L.; Bradshaw, T. D.; Thomas, N. R.
35 Listeria innocua Dps as a nanoplatform for bioluminescence based photodynamic therapy
36 utilizing *Gaussia princeps* luciferase and zinc protoporphyrin IX. *Nanomedicine (N.Y., NY,*
37 *U.S.)* **2019**, *20*, 102005.
38
39 (47) Wick, W.; Platten, M.; Weller, M. New (alternative) temozolomide regimens for the
40 treatment of glioma. *Neuro-oncology* **2009**, *11*(1), 69-79.
41
42
43
44
45
46
47
48
49
50
51
52
53
54
55
56
57
58
59
60

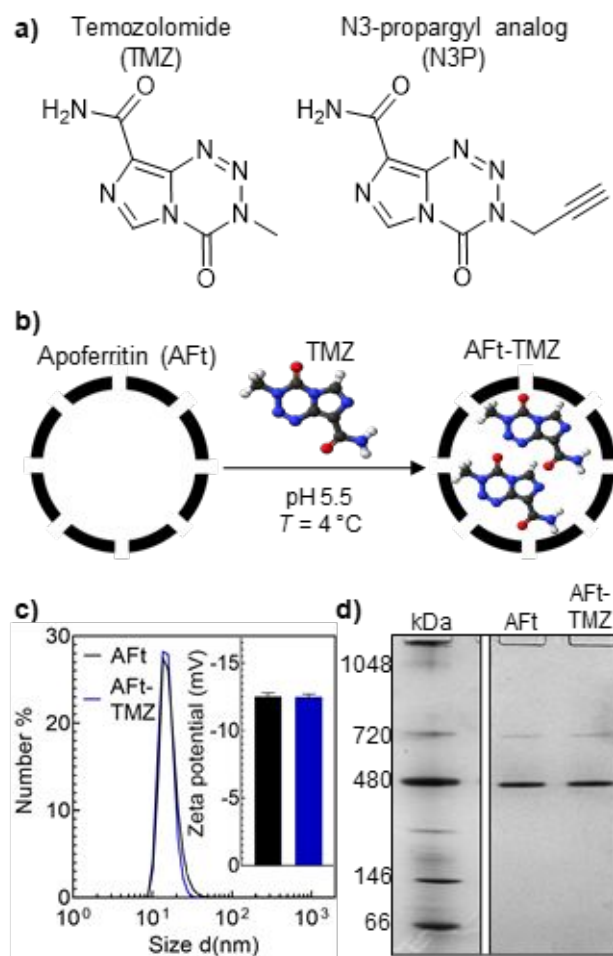


Figure 1. (a) Chemical structures of TMZ and N3P. (b) Illustration of the encapsulation of TMZ into AFt by the nanoreactor route. (c) Hydrodynamic size distribution of AFt and AFt-TMZ measured by dynamic light scattering and (Inset) corresponding zeta potential values. (d) Native-PAGE of AFt and AFt-TMZ performed on a 4-16% gradient gel.

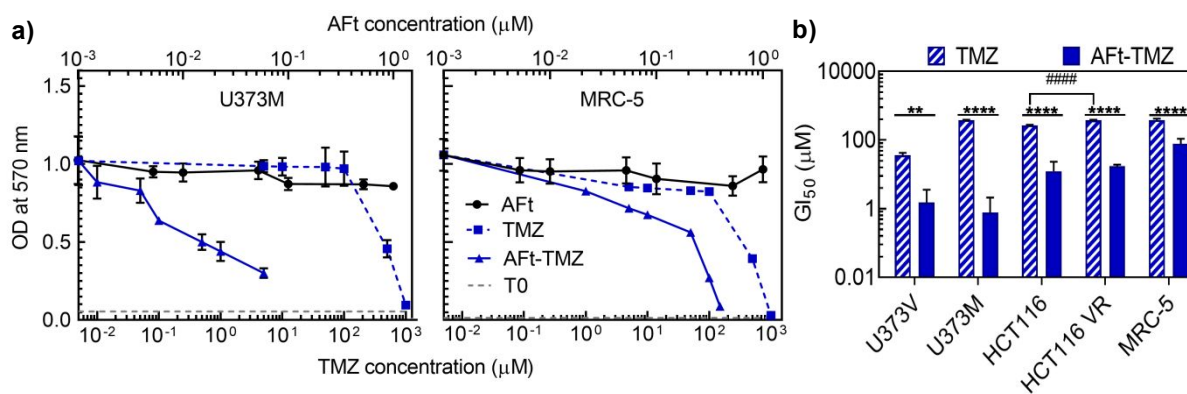


Figure 2. (a) *In vitro* cytotoxicity profiles for U373M (GBM cells, MGMT +) and non-cancerous MRC 5 fibroblasts following 6-day exposure to AFt, TMZ and AFt-TMZ. (b) A summary of GI₅₀ values for TMZ and AFt-TMZ in all studies cell lines. Values are reported as mean ± SD (n > 3). **P < 0.01 and ****P < 0.0001.

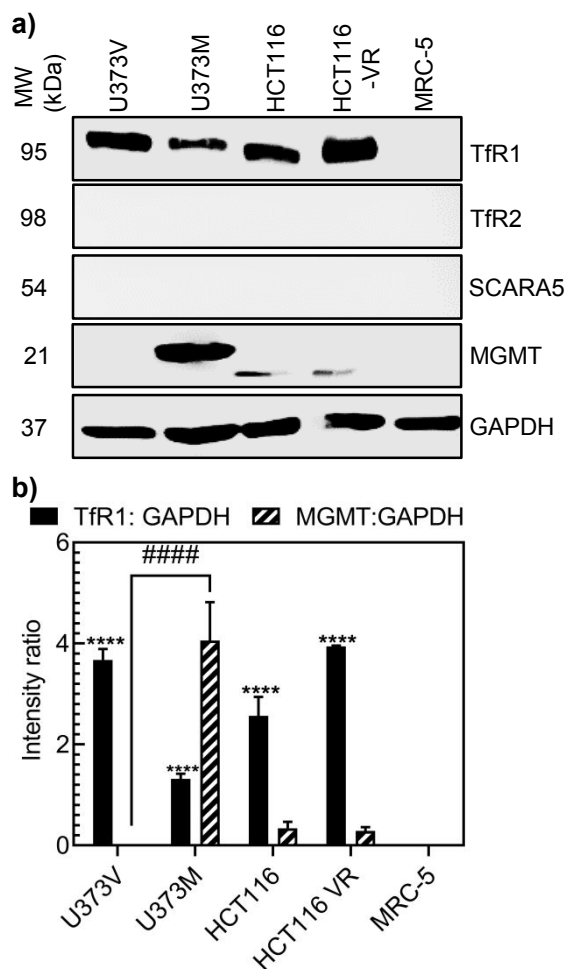


Figure 3. Cellular characterization of protein expression. **(a)** Western blot analysis of membrane bound receptors responsible for AFt uptake and intracellular proteins responsible for TMZ resistance. **(b)** Quantification of target protein band intensity expressed as a ratio of target protein to loading control (GAPDH) band intensity using the LICOR software. Values are reported as mean \pm SD ($n = 3$). Significant difference from MRC-5 are expressed as **** $P < 0.0001$; Significant difference from U373V is expressed as #### $P < 0.0001$.

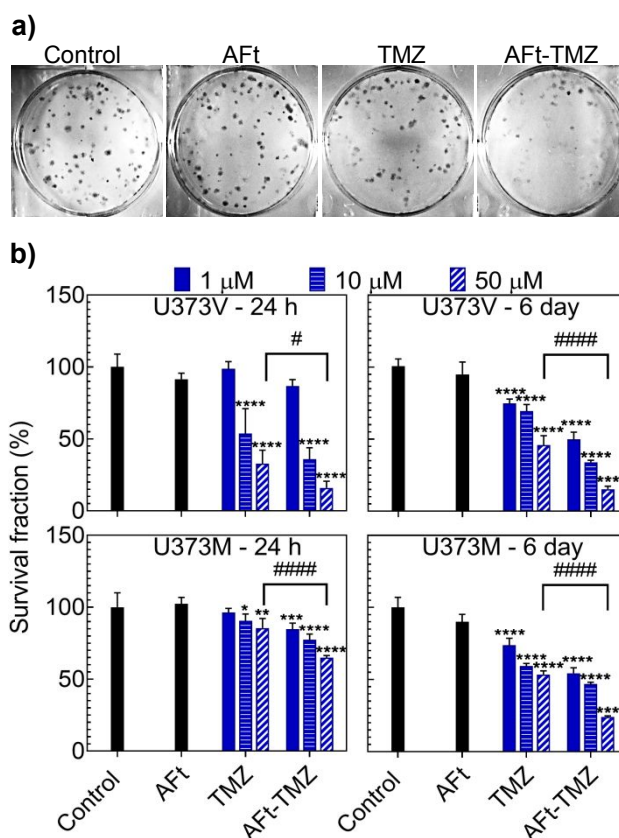


Figure 4. *In vitro* characterization of cell proliferation proficiency following treatment. **(a)** Representative images of the clonogenic assay conducted on U373M for a 6-day treatment (TMZ 50 μM , AFt-TMZ 50 μM , AFt 0.057 μM or media alone) exposure. **(b)** Percentage survival fraction of GBM; MGMT +/- cells following either a 24 h or 6-day treatment regimen with 1, 10 or 50 μM TMZ/ AFt-TMZ and 0.057 μM AFt (equivalent to AFt concentration of AFt-TMZ 50 μM). Values are reported as mean \pm SD (n = 5). Significant difference from the control are expressed as * P < 0.05, ** P < 0.01, *** P < 0.001 and **** P < 0.0001. Significant difference from TMZ are expressed as # P < 0.05. ##### P < 0.0001.

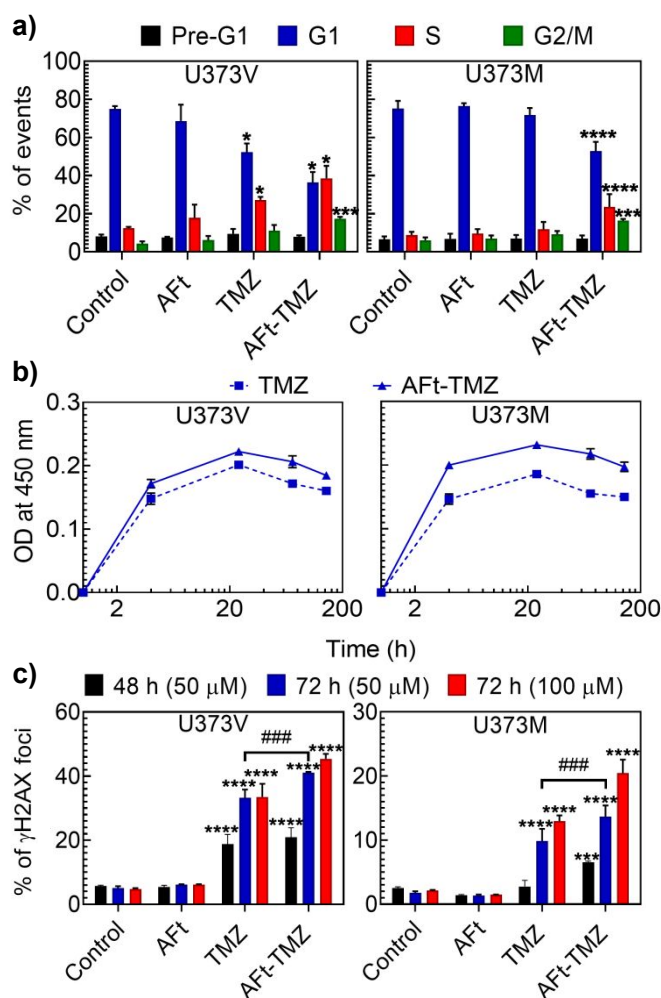


Figure 5. The mechanism of action of TMZ versus AFt delivered TMZ in GBM, MGMT +/- cells. **(a)** Summary of the number of gated events i.e. cells (expressed as a percentage from 10000 gated events), arrested in different phases of the cell cycle after 72 h treatment (TMZ 50 μ M, AFt-TMZ 50 μ M, AFt 0.057 μ M or media alone) exposure. **(b)** ELISA DNA O6-MeG quantification following exposure of cells to 50 μ M of TMZ or AFt-TMZ. **(c)** Summary of the fluorescence intensity of γ H2AX foci (expressed as a percentage from 10000 gated events), after a 48 or 72 h treatment exposure to 50 or 100 μ M of TMZ and AFt-TMZ and 0.057 or 0.1 μ M of AFt. Values are reported as mean \pm SD (n = 3). Significant difference from the control are expressed as * P < 0.05, *** P < 0.001 and **** P < 0.0001. Significant difference from TMZ are expressed as ### P < 0.001.

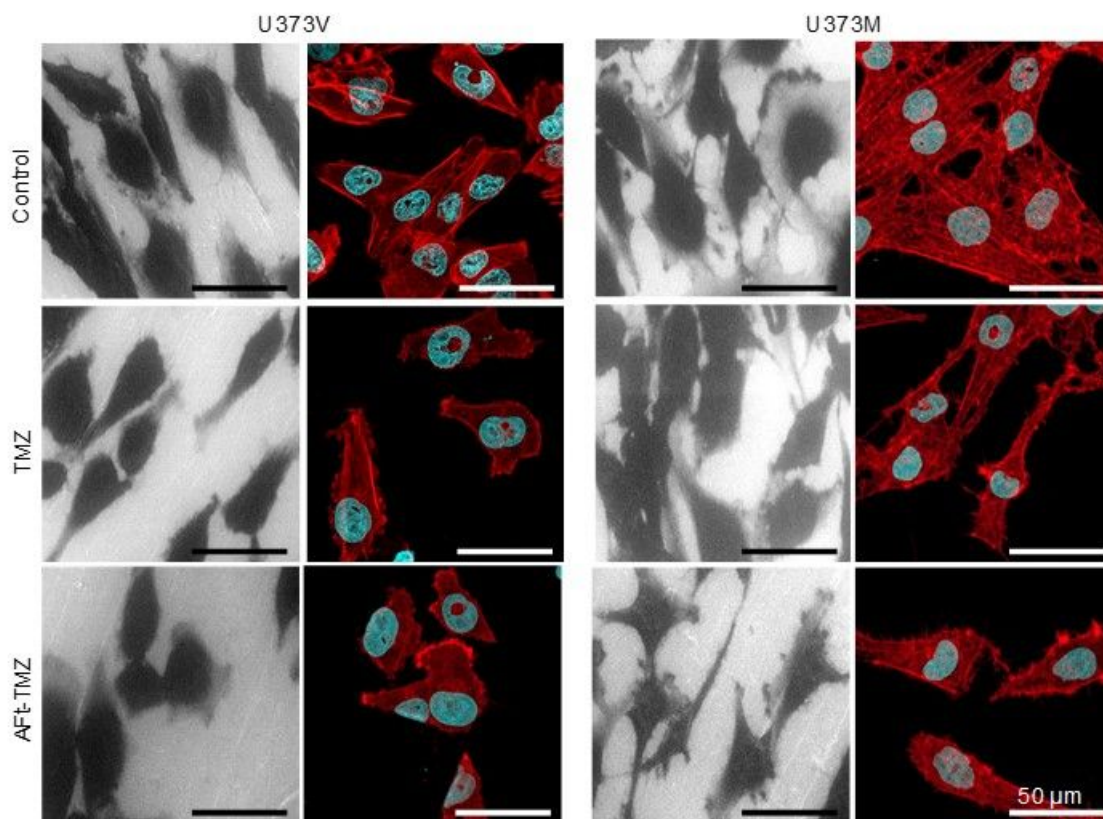


Figure 6. Morphological changes to GBM cells following 24 h treatment exposure (TMZ/ Aft-TMZ 50 μ M). Cell surface morphology was monitored by a combination of ESEM and confocal microscopy (phalloidin (red) - F-actin staining; DAPI (blue) – nucleus staining). Scale bar is 50 μ m.

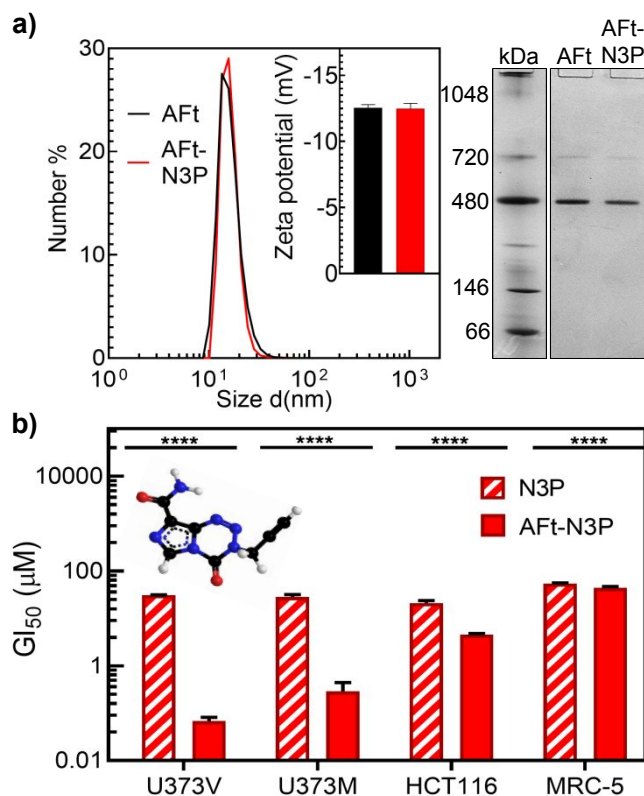


Figure 7. (a) Hydrodynamic size distribution of AFt and AFt-N3P measured by dynamic light scattering and (inset) corresponding zeta potential measurements. In addition, native-PAGE carried out on AFt and AFt-N3P showing protein integrity was performed on a 4-16% gradient gel. (b) *In vitro* cytotoxicity MTT studies with naked and encapsulated N3P (TMZ analog; inset chemical structure shown). Summary of concentration values leading to growth inhibition at 50% (GI₅₀) for test agents against GBM (MGMT +/-), HCT116 (MMR -) and non-cancerous MRC-5 cells. Values are reported as mean ± SD (n=5). ****P < 0.0001.

TABLE OF CONTENTS graphics

